W-band Doppler radar observations of a prescribed fire smoke plume: the EUBURN-FLAMEX 2026 campaign

Franck Donnadieu*[1,2]; Adrien Guyot [3,4]; Julien Delanoë[5]; Frédéric Peyrin[2]

[1] *Université Clermont Auvergne, CNRS, IRD, OPGC, Laboratoire Magmas et Volcans, Clermont-Ferrand, France*
[2] *Université Clermont-Auvergne, CNRS, UAR 833, OPGC, Aubière, France*
[3] *Weather and Climate Science Research Alliance, The University of Queensland, Brisbane, Australia*
[4] *Australian Bureau of Meteorology, Melbourne, Australia*
[5] *LATMOS/IPSL, UVSQ Université Paris-Saclay, Sorbonne Université, CNRS, Guyancourt, France*

**Corresponding author. Email: franck.donnadieu@uca.fr*

Keywords

Doppler radar, smoke plume, dynamics, reflectivity, velocity

Abstract

As climate change increases the frequency, severity, and spatial extent of wildfires, a better understanding of fire dynamics and their environmental consequences is needed. Ground-based radar systems have emerged as a powerful tool for monitoring wildfire smoke, addressing critical challenges in air quality, public health, and fire management. While satellite methods or in-situ sensors often lack the temporal and spatial resolution required to track smoke plumes in real time, Doppler and polarimetric radars fill this gap by detecting and characterizing smoke particles, even in complex atmospheric conditions. In particular, they enable detailed analysis of their structure, particle properties, and atmospheric interactions. Although several studies report radar observations of smoke plumes at S-, X-, and Ka bands, a single study has reported observations of a fire-generated cloud with an airborne W-band radar, and only one has reported a ground-based system looking at the smaller scale dynamics of a prescribed burn smoke plume.

As part of EUBURN multi-year and multi-scale field campaign in Europe, we investigated the ability of a 95 GHz ground-based Doppler radar to detect fire smokes from a prescribed burn on slopy terrain during the FLAMEX 2026 field experiment in Andalusia. Taking advantage of its high sensitivity at millimeter-wave and high temporal and spatial resolutions (25 m, 1 s), we were able to monitor the fire atmospheric emissions at constant slant angle upwind during more than five hours. After heavy rainfall overnight and during the early morning, the burn was ignited on very humid shrubs and soil with progressively drying atmospheric conditions during the day, with the transient occurrence of fog. The pre-fire atmospheric conditions were measured by radio soundings, and the structure of the thick cloud cover was measured by the radar in vertical pointing. During the fire, pulsed atmospheric smoke emissions grew in intensity and could be imaged up to a few kilometres from the radar location. Analysis of the radar reflectivity, Doppler velocities and attenuation constrain the interpretation of the smoke plume dynamics and content, helped by comparison of information on vegetation types and conditions, fire behaviour, meteorological parameters and the emission of gases and aerosols collected by instrumental platforms ran by other teams during FLAMEX 2026.

1. Introduction

Wildfire behaviour is strongly controlled by fine-scale interactions between combustion, turbulence, smoke-plume dynamics, and the surrounding atmosphere. Yet, observing these processes in the field remains challenging because fire plumes evolve rapidly, are spatially heterogeneous, and often occur in environments where conventional meteorological instruments cannot safely be deployed. Remote sensing therefore provides a valuable way to document plume structure and dynamics during experimental fires. Mobile weather radar has been proven to be a very valuable tool for observing these processes (Guyot et al., 2019; McCarthy et al., 2019), with various research teams operating X- or Ka- Band radars in Australia (McCarthy et al., 2018; May et al., 2024) and the US (Lareau et al., 2025; Aydell and Clements, 2023).

In this study, we present what is, to our knowledge, the second use of a ground-based W-band Doppler radar. Tsai et al (2009) reported pulsed W-band radar RHI and PPI scans combined and vertical lidar observations of a prescribed burn smoke plume from 1.6 km downwind. The radar single pulse sensitivity with 1.2 KW power was -26 dBZe at 1 km range. The beamwidth was 0.2°, the spatial resolution 30 m in radial direction and 6 m in azimuthal direction at 2 km, providing very fine pixels in close range. Smoke plume reflectivities in the vicinity of -30 dBZ were measured. Operating at millimetre wavelength, W-band radars are highly sensitive to small ash, smoke, and cloud particles, while its Doppler capability enables measurements of radial velocity within the plume. This makes it particularly suitable for resolving the fine-scale structure of smoke plumes, including vertical motions, turbulent features, and the transition from near-source emissions to the developing convective column. W-band radars are designed as "cloud radars", therefore more susceptible to capture echoes from smaller particles than X-Band or Ka-Band radars.

The radar was deployed during a controlled burn to assess its ability to observe plume morphology and dynamics at high temporal and spatial resolution. We focus on the capability of W-band Doppler radar to capture diluted smoke echoes, retrieve coherent Doppler velocities, and complement existing visual, thermal, and meteorological observations. This first deployment demonstrates the potential of millimetre-wave Doppler radar as a new observational tool for fire-atmosphere interaction studies and for improving our understanding of smoke plume development in controlled and wildfire environments.

2. Methods

2.1. Site and experiment

The prescribed burn was conducted as part of the EUBURN (Denjean et al., 2026) project, an EU-funded collaborative project spanning over multiple research organisations, universities and institutes across European and non-European countries with the aim of observing wildfires and their emissions for prescribed and actual wildfires over the period 2025-2027. This prescribed burn was conducted by the Agencia de Emergencias de Andalucía. The experiment took place on 28 April 2026 in the Sierra de Los Filabres, about 40 km North of Almeria in Andalusia, southern Spain. This international field campaign, hereafter referred to as FLAMEX26, was designed to collect a broad set of measurements before, during, and after the fire. The observing platforms included uncrewed aerial vehicles, in situ measurements within and around the burn plot, and remote-sensing instruments. Vegetation surveys were also conducted before and after the fire.

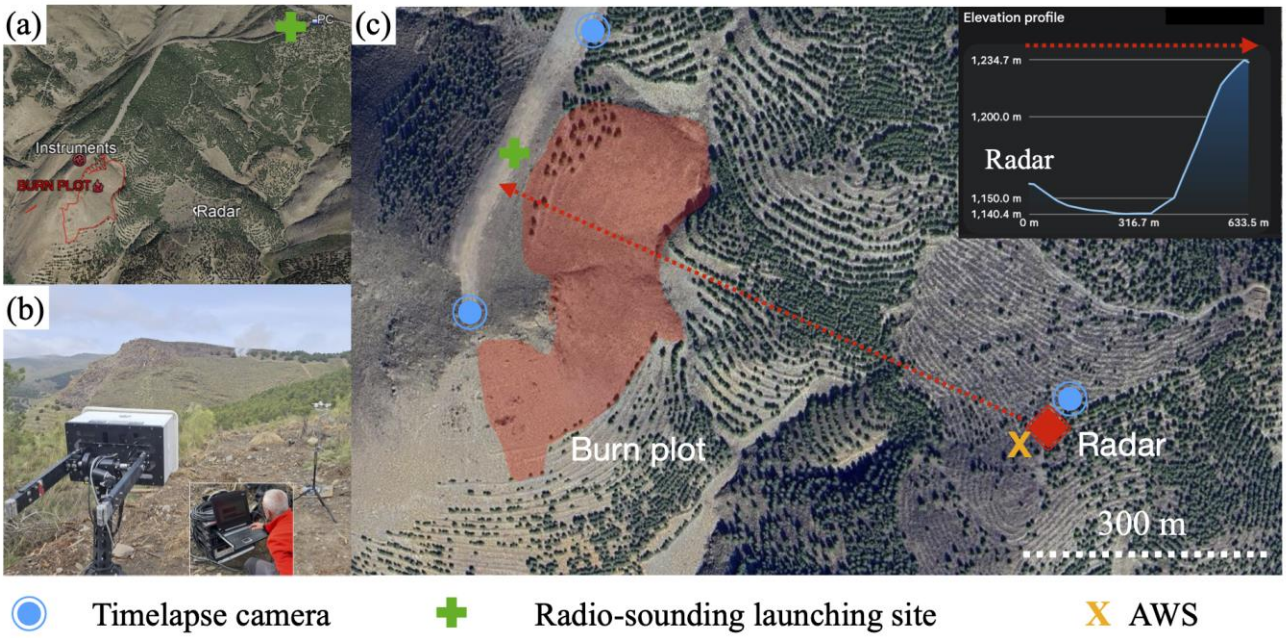

Figure 1 - (a) Location of experimental plot, radar, and command post (PC); (b) The mini-BASTA radar on its motorized tripod aiming obliquely into the smoke plume lofted to the Northwest (NW) above the opposite ridgeline at a distance of approximately 600 m; (c) Experimental plot showing instruments' locations and topographic variations in the aiming direction.

Figure 1 shows the location of the radar in relation to the plot burned. The radar was pointing in azimuth N300, and with a fixed elevation of 10.4°. While the radar has the capability to scan along two axes, this choice of a fully fixed pointing setting was dictated by the fact that the access to the radar was restricted during the full duration of the burn, after ignition was started, therefore rendering changes of scanning strategy on the fly impossible. The radar was located at about 1165 m a.s.l. pointing across a small combe to the WNW above the 4.67 ha burn plot steeply inclined toward the ESE, topped by a NNE-trending ridge at ~1230 m a.s.l., about 650 m from the radar. Ground-level gentle winds were blowing the lofting smoke plume to the NW across the ridge.

Although a small pre-fire was ignited on the ridge at 09:00 UTC to test wind conditions, the main fire was ignited near the plot top center part at 10:00 UTC, then out toward both top sides, and progressively down the sides after 11:00 UTC. Note that foggy conditions appeared for 30 min on the ridge after 11:15 UTC. The most intense smoke emission occured from 12:45 to 13:15 UTC during ignition from the plot bottom part and progression of the fire toward the plot center due to the wind blow from down the combe upward to the NW.

2.2. Instrument and data processing

The radar utilized, namely VOLDORAD-3, is a mini-BASTA adapted from the 95-GHz Bistatic Doppler Radar System for Atmospheric Studies (BASTA) of cloud and fog (Delanoe et al., 2016). Although less sensitive owing to smaller Cassegrain antennas, the mini-BASTA is less cumbersome, lighter and more transportable, therefore easier and quicker to deploy. These advantages are particularly useful to adapt to rough environments and rapidly evolving field conditions. As part of the VOLDORAD instrumental platform of OPGC, this radar is effectively used mainly for the monitoring of short-lived volcanic plumes and ash fallout (Donnadieu et al., 2018; Freret-Lorgeril et al., 2020) in the frame of the National Service for Observation in Volcanology (SNOV, French CNRS-INSU).

The radar transmits a Frequency-Modulated Continuous-Wave at 95 GHz with a power of ~24 dBm into a narrow beam 0.8° in aperture. Its low power consumption around 400 W can be fed by a small 2 KW electric generator. The radar and its positioner mounted on a tripod (for scanning), are controlled by three rack-housed units for power, motorization and processing. Three acquisition modes with 12.5-, 25- and 100-m range resolutions allow the spatial resolution and sensitivity to be adjusted as a function of target distance and reflectivity (typology, size, shape, concentration). These can be acquired in succession (multimode). The integration time, generally 1 s, can also be increased during acquisition or in post-processing to improve sensitivity. Further details on the instrument, receiver chain and signal processing are provided in Delanoë et al. (2016).

For the FLAMEX experiment, the smoke reflectivity from the prescribed burn was poorly known a priori, so we set the intermediate 25 m resolution mode with 1 s integration time. This configuration limits the maximum range to 12 km and the unambiguous velocity to ±9.86 m/s, although moderate aliasing can be post-processed to unfold velocities. The radar acquired data from 08:34 until 14:05 UTC, when the electric generator ran out of gasoline; no operator being allowed on site for safety reasons preventing refueling or ajusting measurement configuration. Record in vertical direction during the first 15 minutes allowed the pre-fire ambiant atmospheric conditions to be characterized, revealing a thick cloud cover (following the heavy overnight and early morning rainfall) spanning from about 4000 to 8500 m a.s.l. with radar reflectivity below 0 dBZ. Along side the radar, a DJI Action Pro camera recorded 2 hours of video, and an Automatic Weather station recorded standard weather variables over the start of the radar scanning period.

3. Results

Figure 2 provides an overview of the W-band radar observations during the burn. The 20 s post integrated reflectivity and Doppler velocity fields show a persistent low-level echo layer below approximately 0.3 km range, and a strong band of ground clutter from the ridge line around the 0.6 km mark, due most likely to second lobe echoes from the signal hitting the ground. Intermittent plume structures extend above this layer.

During the early part of the record, the radar signal is relatively shallow and weak, with most smoke echoes confined to just passed the ridge line, i.e., past the 0.6 km range mark. After approximately 12:00 UTC, the plume becomes progressively more vertically developed and temporally variable, with several pulses of enhanced reflectivity extending to 2–4 km range and occasional echoes reaching beyond 5 km. These pulses are also evident in the Doppler velocity field, where coherent regions of positive and negative velocity indicate rapidly changing motions within the plume in space and time. During the most intense phase, particularly after 13:00 UTC, isolated farther echoes up to 11 km are markedly detected in the same range-time trend as the fire smokes (nearly -10 dBZ at 6 km, Fig.2), including clear detections beyond the range visible in Figure 2. Such isolated detections could arise from the large-scale atmospheric vortices causing the smoke plume to come across the beam at farther distance. The range-time trend provide estimates of the wind speed along-beam component, e.g. ~2 m/s in the first hundred meters beyond the ridge line.

Although no direct Fire Radiative Power (FRP) observations were available, the radar time series provides an indirect view of changes in fire behaviour and particle lofting. Periods of deeper and stronger radar echoes likely correspond to phases of enhanced combustion, increased buoyant forcing, or more efficient entrainment of particles into the plume. These radar-observed phases will be compared with timelapse imagery and derived apparent opacity retrieval (Guyot et al., 2026), Unmanned Aerial Vehicle (UAV) measurements, and in-situ particulate observations conducted near the ridge line, to link radar detectability with independent indicators of plume opacity and smoke loading.

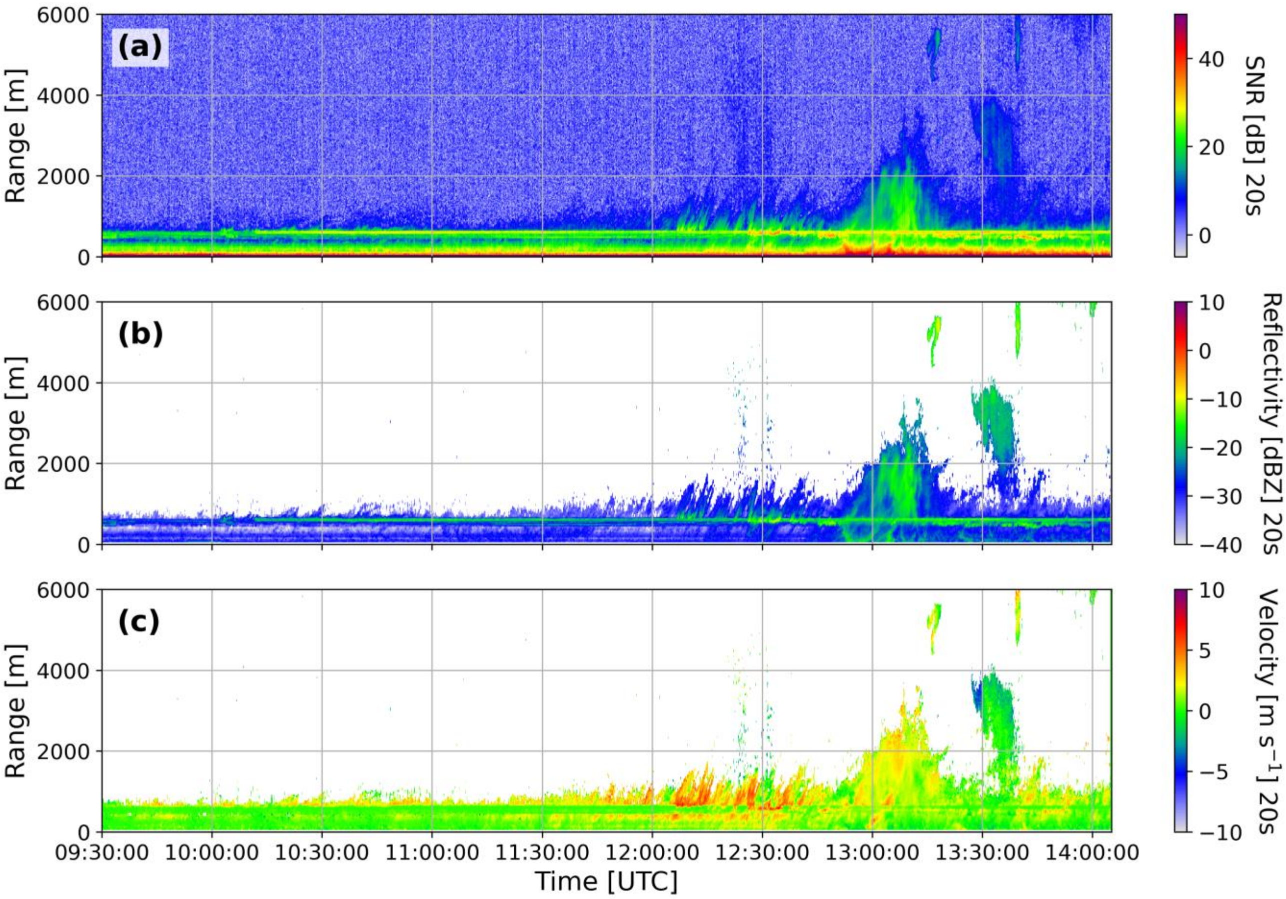

Figure 2 - Time–range evolution of W-band mini-BASTA radar observations during the prescribed burn. (a) 20 s integrated Signal to Noise Ratio [dB], (b) 20 s integrated equivalent reflectivity factor, and (c) 20 s Doppler velocity [m/s]. Only radar gates passing the quality-control mask are shown.

To compare the statistical structure of the native and temporally integrated W-band radar observations, we computed range-dependent frequency distributions of reflectivity and Doppler velocity (Figure 3). These diagrams are analogous to contoured-frequency-by-altitude diagrams, but are expressed as a function of radar range because the instrument was operated in a fixed pointing configuration. At each range gate, valid samples were binned independently and normalised by the number of available observations at that range. This normalisation emphasises changes in the shape of the reflectivity and velocity distributions with range, rather than variations in sampling density.

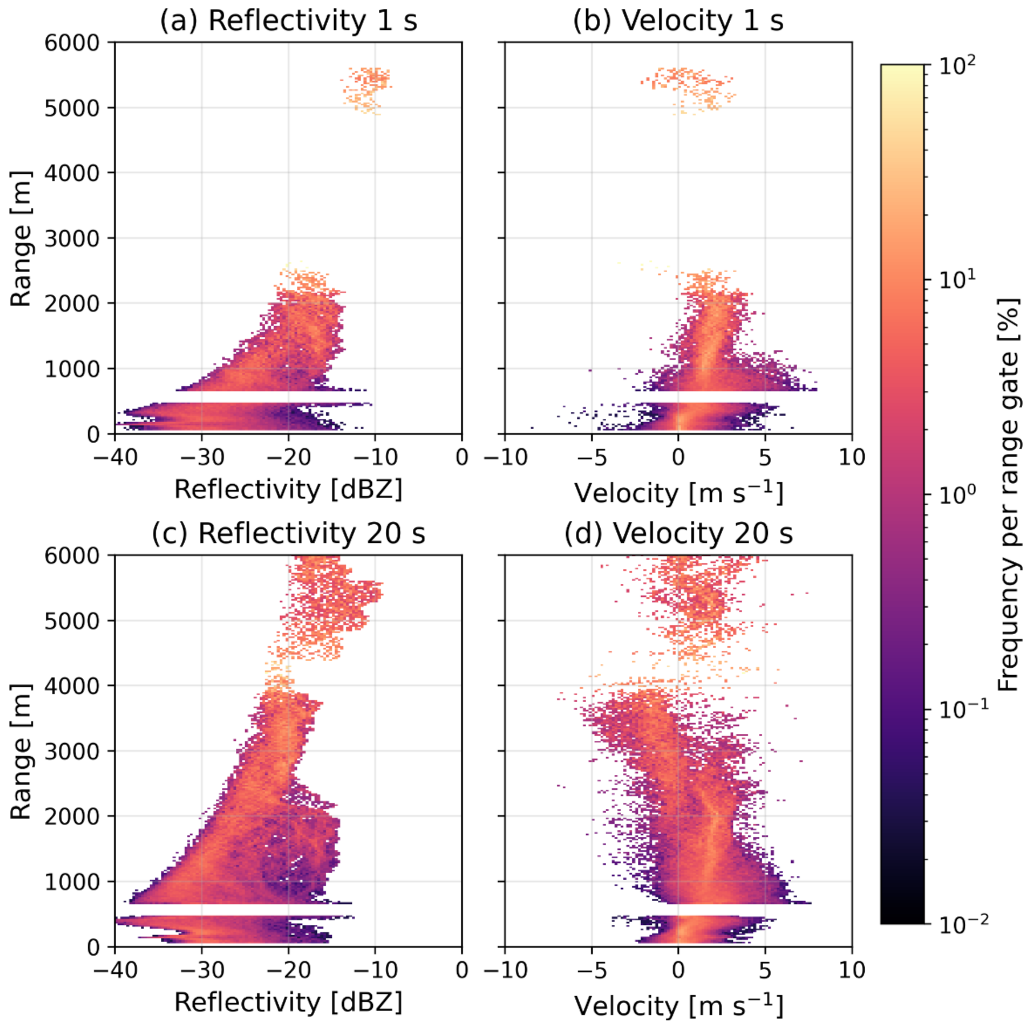

Figure 3 - Range-dependent frequency distributions of W-band radar reflectivity and Doppler velocity before and after temporal integration. Panels show contoured-frequency-by-altitude/range diagrams computed from valid radar samples after 9:30 UTC. Panels (a,b) use the native 1 s observations: (a) reflectivity and (b) Doppler velocity. Panels (c,d) show the corresponding 20 s integrated fields: (c) reflectivity and (d) Doppler velocity. For each range gate, the distribution is normalised by the number of valid samples at that range, so colours represent relative occurrence frequency rather than absolute sample count. The 20 s integration increases echo continuity and reveals more coherent range-dependent structures in both reflectivity and Doppler velocity, particularly above 0.6 km range.

The native 1 s observations show a dominant low-level population below approximately 1 km range, with reflectivity mostly between about −40 and −15 dBZ and Doppler velocity concentrated near weak positive values. After 20 s integration, the distributions become more continuous and coherent in range. The integrated reflectivity distribution highlights the sensitivity versus range of the radar, while the velocity distribution shows a broad range of motions, including coherent positive-velocity structures at low to mid ranges and more variable velocities aloft. This demonstrates that temporal integration reduces sampling sparsity and clarifies the range-dependent organisation of the observed echoes, while retaining the main dynamical signatures present in the native observations.

4. Discussion

The observed range of W-band reflectivity values provides an empirical estimate of the radar detectability threshold for this prescribed-fire plume. This threshold can be compared with independent measures of plume loading, including image-derived apparent opacity (Guyot et al., 2026) and in-situ particulate concentration measured at the ground and by UAV-mounted sensors. Such comparisons will be valuable because they help determine when visually apparent smoke becomes radar-detectable, and whether increases in radar backscatter correspond to enhanced optical opacity or particle concentration. While these measurements are not directly collocated in sampling volume, their combination provides a multi-sensor basis for interpreting the radar signal and for identifying the plume regimes that are detectable by W-band radar. We shall note that for this specific fire, the vegetation moisture content and residual moisture at the soil surface layer was probably high, as the mountain range sustained moderate rainfall on the morning of the burn, which in turn likely produced higher latent heat fluxes from the fire, and a possibly smoke with higher water content compared to a scenario with the absence of rainfall before the burn.

The comparatively low detection threshold of the W-band BASTA radar is a key advantage for observing prescribed-fire plumes. Whereas X- and Ka-band radars are well suited to detecting stronger echoes associated with larger particles, hydrometeors, or intense convective plume cores, W-band measurements are sensitive to weaker backscatter from small particles and tenuous plume structures and better resolved spatially. This makes BASTA particularly useful for medium-size controlled burns, where plume intensity and spatial extent are often too limited for robust detection by conventional scanning weather radars. Rather than replacing lower-frequency systems, W-band observations provide a complementary view of the plume.Moreover, if combined with an X-band radar, which is more sensitive to Bragg scattering, we could isolate the turbulence contribution from smoke backscatter: broadly, X-band also detects changes in the air refractive index, whereas W-band is more sensitive to changes in ash particle size and concentration. This supports a multi-frequency observing strategy in which the different wavelength dependencies of radar backscatter are exploited to constrain particle size and concentration, following approaches developed in volcanic ash radar retrieval studies, including those by Marzano et al. (2006) and colleagues. In fire-plume applications, such a strategy could help distinguish fine ash and small lofted particles from larger firebrands, ash aggregates, or hydrometeor-sized scatterers, while also improving estimates of plume vertical development and particle loading. However, quantitative interpretation of W-band reflectivity must account for attenuation and the strong sensitivity of the signal to particle size, so these observations are best interpreted in combination with complementary sensors and frequencies.

5. Conclusion

This FLAMEX radar deployment demonstrates that W-band Doppler radar offers unique observational capabilities for fire-plume studies, filling an important gap left by previous X- and Ka-band radar applications. Its short wavelength (3.2mm), high sensitivity, and fine spatial sampling make it particularly well suited to detecting weak, diluted smoke plumes from low-intensity fires that may be difficult to observe with longer-wavelength systems. With gate spacing as fine as 25 m, W-band radar can resolve small-scale plume structures and velocity variability close to the source, providing new opportunities to investigate fire–atmosphere interactions across a wider range of fire intensities than previously possible. However, the potential impact of attenuation in dense smoke remains unresolved, as such conditions were not encountered during this experiment. Future observations of more intense fires will be required to assess the operational limits of W-band radar and to determine whether attenuation correction or complementary observations at longer wavelengths are needed.

Acknowledgments

This work is supported by Météo-France, the European Union through the Interreg Sudoe Programme (S2/2.4/F0327), the French National Research Agency through grant agreement no. ANR-24-CE01-3132, the Centre National des Recherches Scientifiques (CNRS) through the program LEFE-INSU, the French National Agency for Space Studies (CNES) and France 2030 via the Centre International des Risques Naturels (Clermont Auvergne Project CIR4). We would like to thank EMA (EMA (Agencia de Seguridad y Gestión Integral de Emergencias de Andalucía) for planning and conducting the burn.

References

Aydell, T. B. and Clements, C. B., 2021. Mobile Ka-band polarimetric Doppler radar observations of wildfire smoke plumes. *Monthly Weather Review*, 149(5), 1247–1264.

Denjean, C. et al., 2026. EUBURN: The southern Europe biomass burning programme. Under review in *Journal of the European Meteorological Society*.

Delanoë, J., Protat, A., Vinson, J.-P., Brett, W., Caudoux, C., Bertrand, F., Parent du Châtelet, J., Hallali, R., Barthes, L., Haeffelin, M. and Dupont, J.-C., 2016. BASTA: A 95-GHz FMCW Doppler radar for cloud and fog studies. *Journal of Atmospheric and Oceanic Technology*, 33(5), 1023–1038.

Donnadieu, F., Freret-Lorgeril, V., Peyrin, F., Hervier, C., Latchimy, T., Rossin, C., Fréville, P., Delanoë, J., Vinson, J.-P., Le Gac, C., Caudoux, C. and Bertrand, F., 2018. First feedback from the use of a portable millimeter-wave radar to characterize volcanic ash plumes. *ACTRIS Cloud Radar Calibration Workshop*, Paris, France, 29–30 November 2018.

Freret-Lorgeril, V., Gilchrist, J., Donnadieu, F., Jellinek, A. M., Delanoë, J., Latchimy, T., Vinson, J.-P., Caudoux, C., Peyrin, F., Hervier, C. and Valade, S., 2020. Ash sedimentation by fingering and sediment thermals from wind-advected volcanic plumes. *Earth and Planetary Science Letters*, 534, 116072. https://doi.org/10.1016/j.epsl.2020.116072

Guyot, A., McGowan, H., Filippi, J.-B., Alonso-Pinar, A., Protat, A., McCarthy, N., Webster, S. and Taylor, A., 2026. Mobile weather radar to provide intelligence on wildfire hazards. *EGUsphere* [preprint]. https://doi.org/10.5194/egusphere-2026-2256

Guyot, A., Donnadieu, F., Paugam, R. and Denjean, C., 2026. VisPanache v1.0: an open-source framework for plume segmentation and apparent opacity retrieval from ground-based timelapse imagery. In preparation for *Geoscientific Model Development*.

Lareau, N. P., Forrest, K. and Clements, C. B., 2025. Counter-rotating vortices during Northern California's 2021 Dixie Fire. *Monthly Weather Review*, 153, 2727–2746. https://doi.org/10.1175/MWR-D-24-0254.1

Marzano, F. S., Barbieri, S., Vulpiani, G. and Rose, W. I., 2006. Volcanic ash cloud retrieval by ground-based microwave weather radar. *IEEE Transactions on Geoscience and Remote Sensing*, 44(11), 3235–3246.

May, P. T., Guyot, A., Protat, A. and Curtis, M., 2024. Accuracy of polarimetric radar ZDR estimates: Implications for the quantitative observation of meteorological and nonmeteorological echoes. *Journal of Atmospheric and Oceanic Technology*, 41(6), 621–628.

McCarthy, N., Guyot, A., Dowdy, A. and McGowan, H., 2019. Wildfire and weather radar: A review. *Journal of Geophysical Research: Atmospheres*, 124(1), 266–286.

McCarthy, N., McGowan, H., Guyot, A. and Dowdy, A., 2018. Mobile X-Pol radar: A new tool for investigating pyroconvection and associated wildfire meteorology. *Bulletin of the American Meteorological Society*, 99, 1177–1195. https://doi.org/10.1175/BAMS-D-16-0118.1

McCarthy, N. F., Guyot, A., Protat, A., Dowdy, A. J. and McGowan, H., 2020. Tracking pyrometeors with meteorological radar using unsupervised machine learning. *Geophysical Research Letters*, 47. https://doi.org/10.1029/2019GL084305

Tsai, P.-S., Frasier, S. J., Goodrick, S., Achtemeier, G. and Odman, M. T., 2009. Combined lidar and radar observations of smoke plumes from prescribed burns. *Proceedings of the Fourth Symposium on Lidar Atmospheric Applications*.